Taylor & Francis
Taylor & Francis Group

RESEARCH PAPER

OPEN ACCESS Check for updates

Dynamics as a cause for the nanoscale organization of the genome

Roman Barth [a], Genevieve Fourel[b,c], and Haitham A. Shaban [d,e]

aDepartment of Bionanoscience, Delft University of Technology, Delft, The Netherlands; bLaboratory of Biology and Modelling of the Cell, University of Lyon, ENS de Lyon, University of Claude Bernard, CNRS UMR 5239, Inserm U1210, Lyon, France; cCentre Blaise Pascal, ENS de Lyon, Lyon, France; dSpectroscopy Department, Physics Division, National Research Centre, Cairo, Egypt; eCenter for Advanced Imaging, Faculty of Arts and Sciences, Harvard University, Cambridge, MA, USA

ABSTRACT
Chromatin 'blobs' were recently identified by live super-resolution imaging of labeled nucleosomes as pervasive but fleeting structural entities. However, the mechanisms leading to the formation of these blobs and their functional implications are unknown. We explore here whether causal relationships exist between parameters that characterize the chromatin blob dynamics and structure, by adapting a framework for spatio-temporal Granger-causality inference. Our analysis reveals that chromatin dynamics is a key determinant for both blob area and local density. Such causality, however, could be demonstrated only in 10–20% of the nucleus, suggesting that chromatin dynamics and structure at the nanometer scale are dominated by stochasticity. We show that the theory of active semiflexible polymers can be invoked to provide potential mechanisms leading to the organization of chromatin into blobs. Our results represent a first step toward elucidating the mechanisms that govern the dynamic and stochastic organization of chromatin in the cell nucleus.

Introduction

The eukaryotic genome is hierarchically structured from the level of nucleosomes over chromatin loops, topologically associated domains (TADs) and phase-separated A/B compartments up to chromosome territories [1]. These structural elements are not static but dynamic entities [2], such that an appreciable heterogeneity between cells [3,4] and in dynamics over time [2,5] exists. Such dynamics is borne out from a host of players interacting with the chromatin fiber, including enzymes that typically use ATP for their function associated with a motion component (polymerases [6], chromatin remodelers, topoisomerases, helicases, cohesins and condensins [7–9] and so on) as well as mere binders, such as HMGB proteins [10] and transcription factors which dynamically induce kinks in the DNA [11]. We will refer to these proteins as 'Active Effectors' in this article. Accordingly, dynamics of the chromatin fiber is altered locally [12–14]., but also globally [15–21], in response to nuclear processes such as

transcription or DNA damage repair. Both dynamics and conformational flexibility are key to allow for long-range communication within a fiber, as involved in innumerable genomics processes and in gene activation by transcriptional enhancers.

Given the observed relationships between structural reorganization of the genome [22,23], nuclear functions and chromatin dynamics, a lasting question in genome biology remains if, and if yes how, chromatin dynamics has an effect on genome organization in nuclear space. To tackle this question, we recently introduced Deep-PALM, a live-cell super-resolution approach able to achieve sub-diffraction spatial resolution and 360 ms temporal resolution to image chromatin *in vivo* [24]. Using Deep-PALM, individual nucleosomes go unseen, and only clustered nucleosomes are eventually detected over the background of super-resolution images, in the form of nanometer-sized 'blobs' (see Figure 1(a)). These clusters manifest indeed as area where the fluorescence is continuous and display forms between

ovoid to oblong with rapidly changing shape, hence the term 'blob'. Each blob likely contains a limited number of nucleosomes (<30, ref. [24,25]) associating transiently within the timescale of about 1 second. The functional implications of blobs remain to be explored.

The ability to obtain time-resolved super-resolution images of chromatin allowed to integrate an Optical Flow approach [20,21], thereby quantifying simultaneously the dynamics, size and distance between chromatin blobs in space and time. These results indicated a strong relationship between the flow magnitude of blobs (i.e. their dynamics) and their local density. Notably, the blob dynamics appear enhanced in regions of high blob density, and conversely isolated blobs in chromatin-void regions appear less mobile.

This and other studies resulted in complex high-dimensional datasets, which reflect stochastic and heterogeneous quantities characterizing chromatin in space and time. In order to allow inferences of relationships in such data, correlations between variables are commonly investigated (Figure 1(b)). While this is a valid approach, one has to be aware of its limitations [26]. In particular, a correlation between variables does not directly imply a causal relationship and in the case that a direct causal relationship indeed exists, it is not clear in which direction. Furthermore, the causality might be indirect, transferred via one or multiple unobserved constituents of a biological pathway (Figure 1(b)). While both correlation and causation can identify which variable preceded the other (Figure 1(b)), a causal relationship is demarcated from a correlation by the fact that
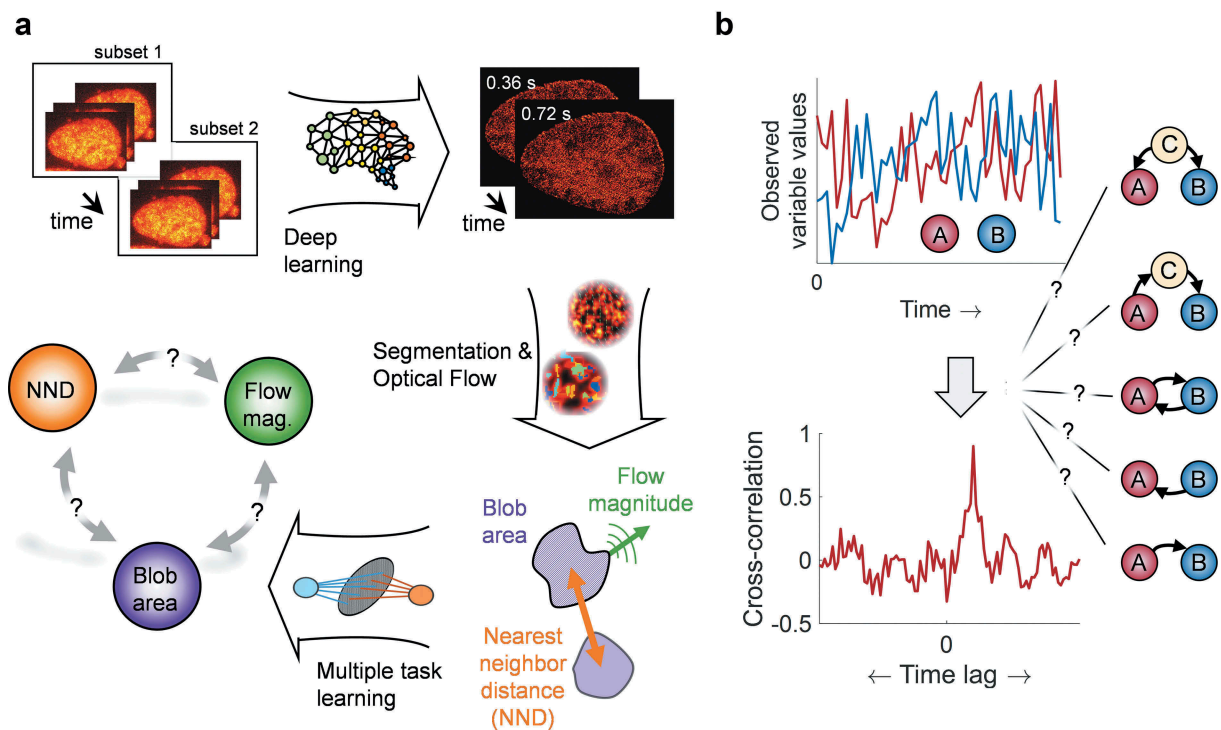

Figure 1. From super-resolution images of fluorescently labeled chromatin to Granger-causal inference between its structure and dynamics. (a) Human osteosarcoma U2OS expressing H2B-PATagRFP cells were imaged. Deep-PALM combines the predictions of a deep learning algorithm from a subset of 12 images to reconstruct a super-resolved image of chromatin with a temporal resolution of 360 ms at 63 nm spatial resolution [24]. Segmentation of chromatin blobs and Optical Flow analysis allows ascribing a nearest neighbor distance (NND), blob area and flow magnitude to each blob in each frame individually. Finally, to infer a Granger-causal relationship between these characterizing parameters, multi-task learning is employed. (b) Whether two observed stochastic variables (a) and (b) are operationally related may be tested by computing a cross-correlation between those variables. The time lag between the variables can be inferred from the absolute maximum value of the cross-correlation curve. However, such a correlation analysis cannot reveal whether the relationship involves causation and in which direction causality is present. Some of the simplest scenarios in a biological context are depicted (from top to bottom): (a) causes (b); (b) causes (a); (a) and (b) are in a feedback loop; (a) causes (b) indirectly via (c); (c) is the common cause of both (a) and (b).

the past of the cause influences the future of the effect in a way that no other measured variable does, including the effect itself. Noteworthy, while correlation analysis can only be carried out pairwise, causal relationships can be inferred among several variables.

The inference of a causal relationship (the inference of a directed information flow) is thus more powerful than the observation of a correlation alone, especially in complex systems such as the genome. A methodology to infer causal paths between the chromatin structure, dynamics and ultimately function is therefore highly desired, but difficult to obtain. The exploration of true causal relationships would indeed require the complete knowledge of the system, in the sense that every possible influence on genome structure and dynamics (proteins, nuclear morphology, etc.) should be mapped at sufficiently high resolution in three-dimensional space and time. Although approached using simple organisms, absolute complete knowledge of a living system is still virtually impossible [27] as one can hope to simultaneously capture only a few out of the vast spectrum of parameters at best. The concept of Granger-causality [28] circumvents this issue by inferring Granger-causal relationships only among a subset of experimentally observable variables. In particular, the analysis of Granger-causality is based on the identification of essential variables (the cause) to predict a target variable (the effect). While both correlation as well as causality analyses suffer from the presence of unobserved variables, identification of causal relationships even among the limited subset of observable variables in a system can, however, indicate which variable is a cause and which one is an effect (possibly via a yet to be discovered pathway). Here, we adapt the abstract concept of Granger-causality to the analysis of Granger-causal relationships between chromatin dynamics and structure at the nanometer scale using the unique data set of our recent chromatin live-cell super-resolution imaging based on deep learning (Deep-PALM) [24]. We use the chromatin blob flow magnitude as a measure of local chromatin dynamics and the blob nearest neighbor distance (NND) as well as the blob area as structural parameters. Our analysis revealed a unidirectional Granger-causality from flow magnitude to both blob NND and blob area, in pixels representing about 10% to 20% of the nuclear volume. We discuss these findings in the light of the theory of active polymers and we further reason that the pervasive activity of Active Effectors on the chromatin fiber may qualitatively and quantitatively explain (i) why chromatin blobs exist and (ii) how chromatin dynamics may influence their structure with respect to inter-blob contacts.

Materials and methods

Cell culture

U2OS expressing H2B-PATagRFP cells were cultured in DMEM (with 4.5 g/l glucose) augmented with 10% fetal bovine serum (FBS), 100 μg/ml penicillin, 2 mM glutamine, and 100 U/ml streptomycin were incubated at 37°C and in 5% CO_2. Cells were plated 24 hours before imaging on 35 mm Petri dishes with a #1.5 coverslip like bottom (ibidi, Biovalley) with a density of 2×10^5 cells/dish. Shortly before imaging, the growth medium was replaced by Leibovitz's L-15 medium (Life Technologies) supplemented with 10% FBS, 100 μg/ml penicillin, 2 mM glutamine and 100 U/ml streptomycin.

PALM imaging

The Deep-PALM imaging conditions are described in our recent publication [24]. Briefly, a fully automated Nikon TI-E/B PALM (Nikon Instruments) microscope equipped with incubator was used for live cell imaging. NIS-Elements software was used for acquiring the images at 30 ms per frame. PATagRFP was illuminated using a laser line of 561 nm (~50–60 W/cm^2 at the sample) along with the 405 nm laser line for photo-activation (~2–2.5 W/cm^2 at the sample). Excitation wavelengths were merged into a TIRF oil immersion objective (1.49 NA, 100x; Nikon). The same objective was used for collecting the fluorescence emission signal and spectrally filtered by a Quad-Band beam splitter (ZT405/488/561/647rpc-UF2, Chroma Technology) with Quad-Band emission filter (ZET405/488/561/647 m-TRF, Chroma). Then, the signal was recorded on an EMCCD

camera (Andor iXon X3 DU-897, Andor Technologies) with a pixel size of 108 nm.

Deep-PALM analysis and image processing

Super-resolution images were obtained using a custom-trained convolutional neural network (CNN, ref. [29]) with an effective pixel size of 13.5 nm. Individual chromatin blobs were segmented using an adapted marker-assisted watershed algorithm and the blob centroid position and area were computed. Using additionally Optical Flow to reconstruct flow fields of chromatin [20,21], each blob was ascribed three parameters: its area, its nearest neighbor distance (NND) and its (instantaneous) flow magnitude. In order to retrieve a gridded representation of all variables, the variables were subsequently interpolated onto a fivefold down sampled pixel grid, resulting in an effective pixel size of 67.5 nm. Details on the super-resolution reconstruction as well as on the segmentation and dynamic analyses can be found in [24].

A framework for the inference of Granger-causality in spatio-temporal data

Granger-causality is assessed between a target variable Y and an input variable X_1, potentially conditioned on one or several common variables X_2, X_3, etc. of the system. We observe each variable at each grid point l (i.e. pixel) across the entire nucleus and at each time point t. The target variable at location l is denoted $Y^{(l)} = \{Y_1^{(l)}, Y_2^{(l)}, \dots Y_T^{(l)}\} \in \mathbb{R}^{\mathrm{T}}$, where T is the number of time points. Here, $T = 166$, covering a total of $\tilde{6}0s$ with a time resolution of $\Delta t = 360ms$. Similarly, $X^{(l)} = \{X_1^{(l)}, X_2^{(l)}, \dots X_T^{(l)}\} \in \mathbb{R}^{\mathrm{Txd}}$, where $X_t^{(l)}$ is a tupel of the cause variable $X_{1t}^{(l)}$ and the $d-1$ conditional variables $X_{2t}^{(l)}, \dots, X_{dt}^{(l)}$, etc. at location l and time t. d thus denotes the number of input variables, including the potential cause. As stated in the main text (Figure 2(a)), testing for Granger-causality involves modeling of the target Y using the lagged variables X (ref. [28]). The base model excludes the variable X_1 for which Granger-causality is tested:

$$Y_t = \widehat{Y}_t + \epsilon_t$$
$$= w_{00} + \sum_{p=1}^{P}\left(w_{0p}Y_{t-p} + \sum_{n=2}^{d} w_{np}X_{n,t-p}\right) + \epsilon_t, \quad (1)$$

where $\widehat{Y}_t$ is the model prediction of the true target Y_t, ϵ_t is a residual noise term, the matrix w_{ij} denotes the coefficients of the base model and P is the maximum time lag considered. The full model contains all explicit and conditional cause variables $X_1, \dots, X_d$:

$$Y_t = \widehat{Y}_t + \epsilon_t$$
$$= w_{00} + \sum_{p=1}^{P}\left(w_{0p}Y_{t-p} + w_{1p}X_{1,t-p} + \sum_{n=2}^{d} w_{np}X_{n,t-p}\right)$$
$$+ \epsilon_t \quad (2)$$

Note that the second sum runs from 2 to d in the base and the full model and the contribution of the cause-variable X_1 is written explicitly in the latter. Granger-causality from X_1 to Y is present if the predictions $\hat{Y}$ of the full model (including the past value of X_1) are significantly better than those of the base model. Quantitatively, we assess the significance in two complementary ways. First, we use the Diebold–Mariano test [30] to evaluate if the predictions of the two models are significantly different. Then, we compute the adjusted R^2 value to account for the varying number of coefficients in the base and full model [31]:

$$R_{adj}^2 = 1 - \left(1 - R^2\right)\frac{N-1}{N-k-1}, \quad (3)$$

where N is the total number of samples, k is the number of parameters in the model and R^2 is the coefficient of determination:

$$R^2 = 1 - \frac{\sum_{t=P+1}^{T}\left(Y_t - \widehat{Y}_t\right)^2}{\sum_{t=P+1}^{T}\left(Y_t - \overline{Y_t}\right)^2}, \quad (4)$$

with $\overline{Y}$ denoting the time average. Pixels at which the adjusted R^2 of the full model is negative or the Diebold–Mariano test does not indicate a significant difference between the prediction errors of full and base models are marked as non-causal.

Multi-task learning

We aim to solve regression problems of the form of Equations (1) or (2) in order to find the matrix
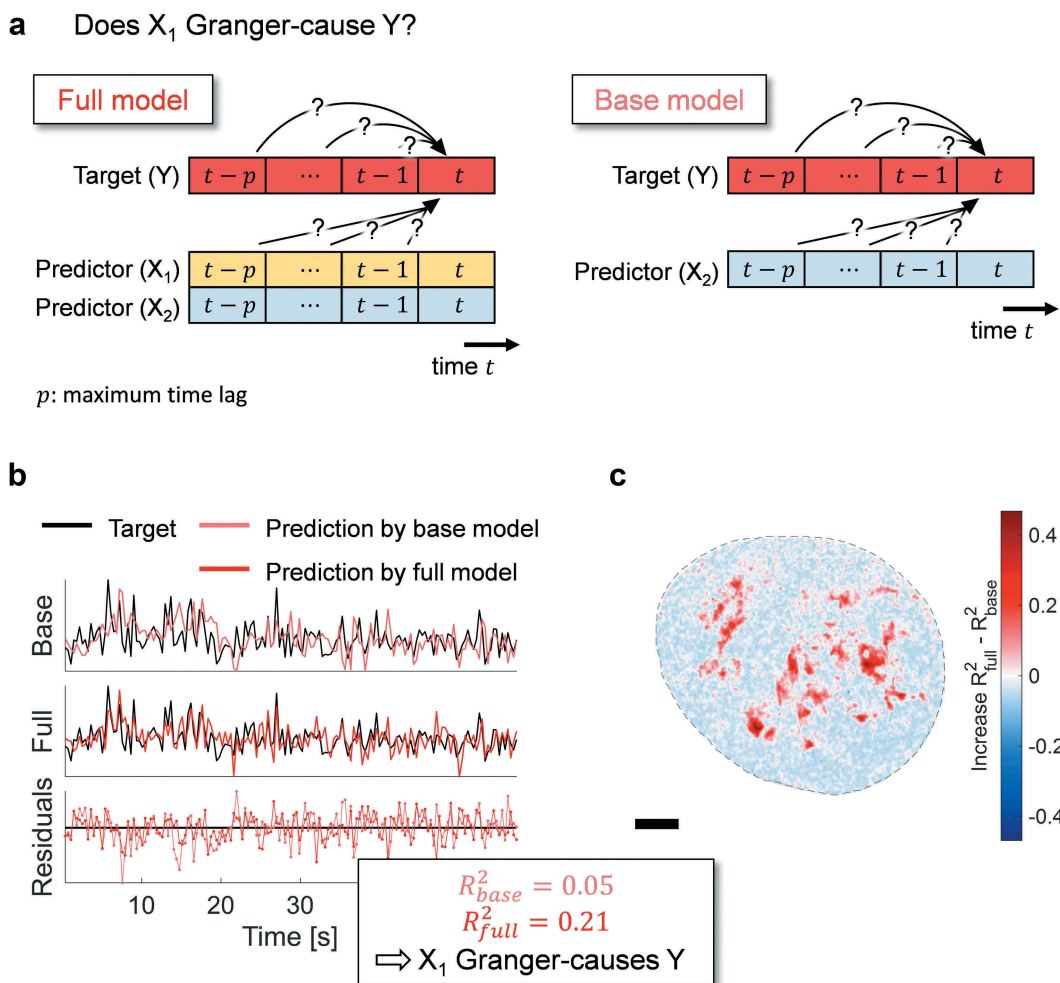
Figure 2. Inference of Granger-causality. (a) The value of a target variable Y at time t may be determined by its own past and the past values of other variables in the system X_1 and X_2. The full model (left panel) consists of a linear relationship between the values of Y, X_1 and X_2 from the time point $t - p$, where p indicates the maximum time lag considered, to time point $t - 1$. In contrast, the base model takes only variables Y and X_2 into account (right panel). (b) Both models are independently optimized to model the target Y and their prediction accuracy is assessed by computing the adjusted R^2 via their residuals. If and only if the adjusted R^2 value of the full model is positive, higher than of the base model and the Diebold-Mariano statistic is significant (Materials and Methods), X_1 is said to Granger-cause Y. In the depicted example, Y is the blob NND at a chosen pixel within the nuclear interior. All time traces have been scaled to mean zero and unit variance. (C) An exemplary map across a nucleus showing the difference between the adjusted R^2 values of the full and the base model. The target variable is the blob NND. Positive values (red) indicate that the variable under consideration (here X_1) considerably improves the modeling of Y and therefore Granger-causes Y, while negative values (blue) indicate that no Granger-causality can be detected during the time of the observation.

w. This can be done for each pixel individually by minimizing a loss function Ψ:

$$\min_{\{w^{(1)},\ldots,w^{(L)}\}} \sum_{l=1}^{L} \sum_{t=1}^{T} \Psi\left(w^{(l)} X_t^{(l)}, Y_t^{(l)}\right), \quad (5)$$

where L is the number of locations. However, it was shown previously that chromatin dynamics [20,21] as well as the chromatin structure [24] is spatially correlated. It is, therefore, reasonable to exploit the fact that different locations share a similar behavior.

We, therefore, use multi-task learning, following an earlier approach to fit linear regression models to spatially correlated time-series in the geoscience domain [32]. In this work, the authors use an alternative structure optimization (ASO, ref. [33]) method in order to simultaneously learn a shared low-dimensional representation among the tasks. In particular, the weight matrix w is split into two parts: $w = u + v\Theta$, where u is a weight matrix in the original d-dimensional space, v is a weight matrix in the shared low-dimensional space and Θ is

a parameter matrix with orthonormal row vectors ($\Theta\Theta' = 1$). The ASO multi-task learning optimization can be thus expressed as

$$\min_{\{w^{(1)},\ldots,w^{(L)}\},\Theta\Theta'=1} \sum_{l=1}^{L}\left(\sum_{t=1}^{T}\Psi\left(w^{(l)}X_t^{(l)}, Y_t^{(l)}\right) + \lambda||u^{(l)}||_2^2\right), \quad (6)$$

With the regularization term $u^{(l)2}_2$ and a regularization parameter λ. This term penalizes weight differences between the high-dimensional and low-dimensional space, parametrized by Θ. A memory-limited Broyden–Fletcher–Goldfarb–Shanno (L-BFGS) algorithm [34] is used to optimize Equation (6). Here, we use a maximum time lag of 3.6 s (10 data points) for the regression, which allows for the incorporation of reasonably long time scale in the inference, while the number of optimizable parameters remains feasible (given time series consisting of 166 data points). The number of parameters equals the number of variables in the system times the number of time points (three variables times 10-time lags in this case). Further details on the regression can be found in [32].

The multi-target learning algorithm uses the information of spatially related processes and therefore enhances its prediction accuracy [32]. The resulting weight matrix w is used to construct the model predictions $\widehat{Y}_t^{(l)} = wX_t^{(l)}$, which are used to evaluate the prediction performance of the base and full model in terms of R^2_{adj}.

Results

A framework to infer Granger-causality between chromatin dynamics and structure

The probability that a true causal relationship with all of the engaging components can be established in a biological experiment is very small – usually, only a subset of all potential direct, indirect or hidden variables can be observed (see the indirect causal relationships via an unobserved component 'C' in Figure 1(b)). We decided therefore to employ the concept of Granger-causality to deduce the causal relationship between chromatin structure and dynamics [28]. Briefly, a time series X_1 is said to Granger-cause Y, given another observable time series X_2 inherent in the system, if the past values of X_1, X_2 and Y can predict Y at the current

time t better than X_2 and Y alone. This definition can be extended to include additional observable time series in the system apart from X_2 if such data become available. However, since our data set comprises three variables of interest, we stick to one target, one predictor and one conditional variable for simplicity. The concept is illustrated in Figure 2(a). A basic principle of causality is that there is no instantaneous influence of the cause to the effect. Instead, the value of Y at time t can be modeled as a linear superposition of past values of X_1, X_2 and Y up to a maximum time lag considered (for details on the model regression strategy, see Materials and Methods). This constitutes the 'full' model, in which all observed system variables are taken into account (Figure 2(a); left). In contrast, the 'base model' uses only past values of the common variables X_2 and Y (Figure 2(a); right). The prediction accuracy of both models is then evaluated using the residuals between the predicted and true values of Y at time t (Figure 2 (b)) and quantified using the adjusted R^2 value. Additionally, a Diebold–Mariano test is used to consider only significant differences in the prediction accuracy of the two models (Materials and Methods). The full and base models are evaluated at all pixels within the nucleus. Pixels at which the adjusted R^2 value of the full model is higher than of the base model indicate pixels at which a Granger-causal relationship can be detected (Figure 2(c)).

While this framework is not able to address head-on the true causality for a system as complex as a human cell (the current state-of-the-art experimental data do not allow to do so), it is able to infer relative causalities (Granger-causalities) among the set of accessible parameters. The detection of Granger-causality thus indicates that some path exists from one variable to another such that the latter appears to arise as a consequence of the former. Compared to a correlation analysis, inference of Granger-causality notably adds information about the direction of influence, and hence makes it possible to classify two variables as cause and effect. However, it is not possible to directly analyze which molecular constituents of the system are involved and which pathway is responsible for the observed causality. The framework presented here,

therefore, represents a first step toward a more extensive inference of causal relationships in the highly complex context of chromatin in space and time. Moreover, it opens avenues to truly identify and decipher the mechanisms responsible for dynamic and functional chromatin organization in the future.

Chromatin dynamics act upstream of blob density

We imaged H2B-PATagRFP in live human bone osteosarcoma (U2OS) cells for up to 60 seconds using Deep-PALM, a live chromatin super-resolution technique [24]. H2B is one of the four core histones found in every nucleosome, and imaging H2B-PATagRFP thus constitutes a way to follow the motion of chromatin in a nucleus.

We analyzed a series of 166 super-resolved frames of dynamic chromatin with a time resolution of 360 ms, governing ~60 seconds and a spatial resolution of 63 nm. Segmentation of the spatially heterogeneous H2B signal identified ~10,000 chromatin 'blobs' at any time in a U2OS nucleus (Figure 1(a)). The blobs appear to result from the dynamic and stochastic association of a number (<30) of nucleosomes in groups [24,25]. While blobs assemble/dissociate on the time scale of about 1 s, blobs are likely to be identified with sub-TADs in the time-average limit [24]. However, the functional or physical mechanisms that determine their formation and characteristics are yet unknown. Chromatin blobs were experimentally characterized in terms of their area, axial dimensions (45 to 90 nm wide elongated shape) and their nearest neighbor distance (NND) between each other [24]. Analysis of the apparent bulk chromatin motion across the image series using Optical Flow [20,21] allowed moreover to ascribe an instantaneous flow magnitude (velocity) to each blob (Figure 1(a)).

We applied the framework introduced above to these three parameters characterizing chromatin dynamics (the instantaneous flow magnitude) and organization (the NND between blobs and the blob area). The three parameters could potentially exhibit causal relationships in any direction and also participate in feedback loops (Figure 1 (b)). We, therefore, tested all possible combinations for Granger-causal relationships. Pixels at which Granger-causality was detected within an exemplary nucleus are marked by the respective color of the cause (Figure 3(a)). In general, when Granger-causality was detected, it was observed in no more than 20% of the nucleus suggesting a picture where stochasticity dominates over order. Remarkably, the flow magnitude appears to act upstream and determine the NND and blob area, while the inverse relationship was hardly ever observed (<1%). This indicates that chromatin dynamics is a key determinant of chromatin organization at the nanoscale. Such Granger-causal relationships could be demonstrated in essentially non-overlapping areas of the nucleus for each parameter. That dynamics is Granger-causal for the blob density was observed in large micrometer-spanning, connected regions and mostly in the nuclear interior (Figure 3(b)). In contrast, dynamics was found to be a Granger-cause for the observed blob area in smaller regions and rather closer to the nuclear periphery (Figure 3(b)). The NND and blob area further appear connected in a feedback loop in pixels scattered throughout the nucleus, suggesting they are Granger-cause and effect of each other. A causal loop diagram shows the direction of the observed Granger-causalities and highlights that these Granger-causal relationships could be demonstrated in ca. 10% of pixels in every case (Figure 3(c)). A possible scenario could, therefore, be that the diagram applies to chromatin in general but can only be demonstrated when and where order outweighs stochasticity for a given parameter. Another reason would be that we can currently only inspect temporal but not spatial Granger-causality between neighboring pixels due to technical limitations. The fraction of pixel for which we can demonstrate Granger-causality, therefore, appears as a lower bound.

For the cases, in which causal relationships could be identified, we analyzed the (temporal) regression weights for the target, predictor and conditional variable nucleus-wide (Supplementary Figure 1(a)). The temporal weights indicate the relevance of a variable at time $t - \Delta t$ to predict the target variable at time t, where Δt is a time lag. Concomitantly, the temporal cross-correlation between target and predictor or target and conditional variable, respectively, is shown for
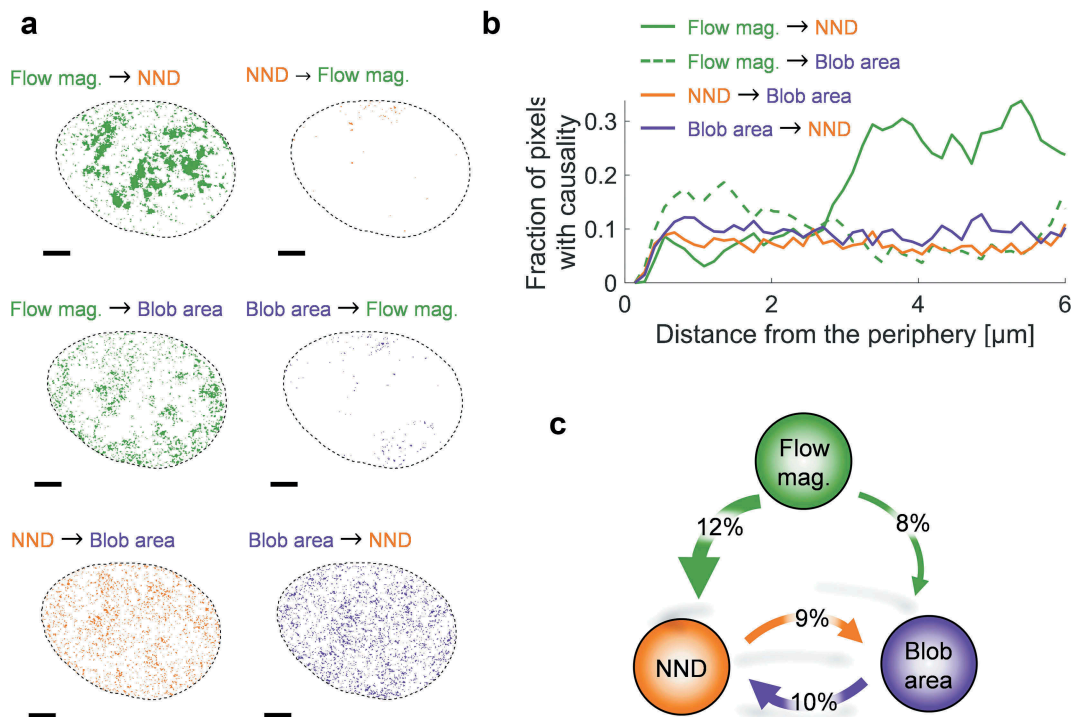
Figure 3. Chromatin flow magnitude Granger-causes chromatin structure. (a) All combinations between potential Granger-causal relationships of the system variables were tested. An exemplary nucleus is shown for which pixels are colored according to the cause. The flow magnitude (green) is shown to mainly cause structural parameters to vary, while the inverse was barely observed. Scale bar is 3 μm. (b) The fraction of pixels for which Granger-causality was observed is shown in dependence of the distance to the nuclear periphery. (c) A loop diagram summarizing the Granger-causal relationship between the flow magnitude, NND and blob area. Percentages correspond to the average frequency across the data set at which pixels were detected with a Granger-causal relationship in the indicated direction, relative to the nucleus size. Percentages <2% were omitted for clarity.

the first 10 time lags (3.6 seconds in total; Supplementary Figure 1(b)). In general, blob NND and area exhibit an inverse relationship in both the regression weights and the temporal cross-correlation (see below). The influence of the flow magnitude on the regression is largest when the flow magnitude is identified as the cause of a structural parameter and almost negligible otherwise, as expected (Supplementary Figure 1(a)). In contrast, the cross-correlation between flow magnitude and either NND or area (Supplementary Figure 1(b)) differs from zero for the considered time lags irrespective of the identified causality. This demonstrates that a causal relationship between two variables does not necessarily exist, even when the parameters are correlated. It is likely that the correlation is established via one or multiple unobserved factor(s).

We next examined whether individual parameters showed any noticeable deviations in regions in which Granger-causality could be demonstrated as compared with the rest of the nucleus. The

dynamics was found to be higher and blobs were, on average, closer in regions in which the flow magnitude was shown to act upstream of the blob density (Figure 4(a–c)). This finding is in line with a correlation approach that previously found that blobs with close neighbors are on average more dynamic than blobs further away from each other [24]. Here we extend this observation by noting that blobs arise with a higher density actually as a consequence of locally elevated dynamics in such nuclear regions. In contrast, the flow magnitude appears overall similar for pixels in which the flow magnitude could be demonstrated to be a cause for the blob surface area, as compared with the rest of the nucleus (Figure 4(e)). In these restricted regions, however, blobs tended to be smaller and blob density was clearly lower on average (figure 4(f,g)), an inverse trend as compared with regions in which flow magnitude was shown to act upstream of blob density. Regarding the Granger-causal loop involving only the NND and blob area, no significant bias in any parameter
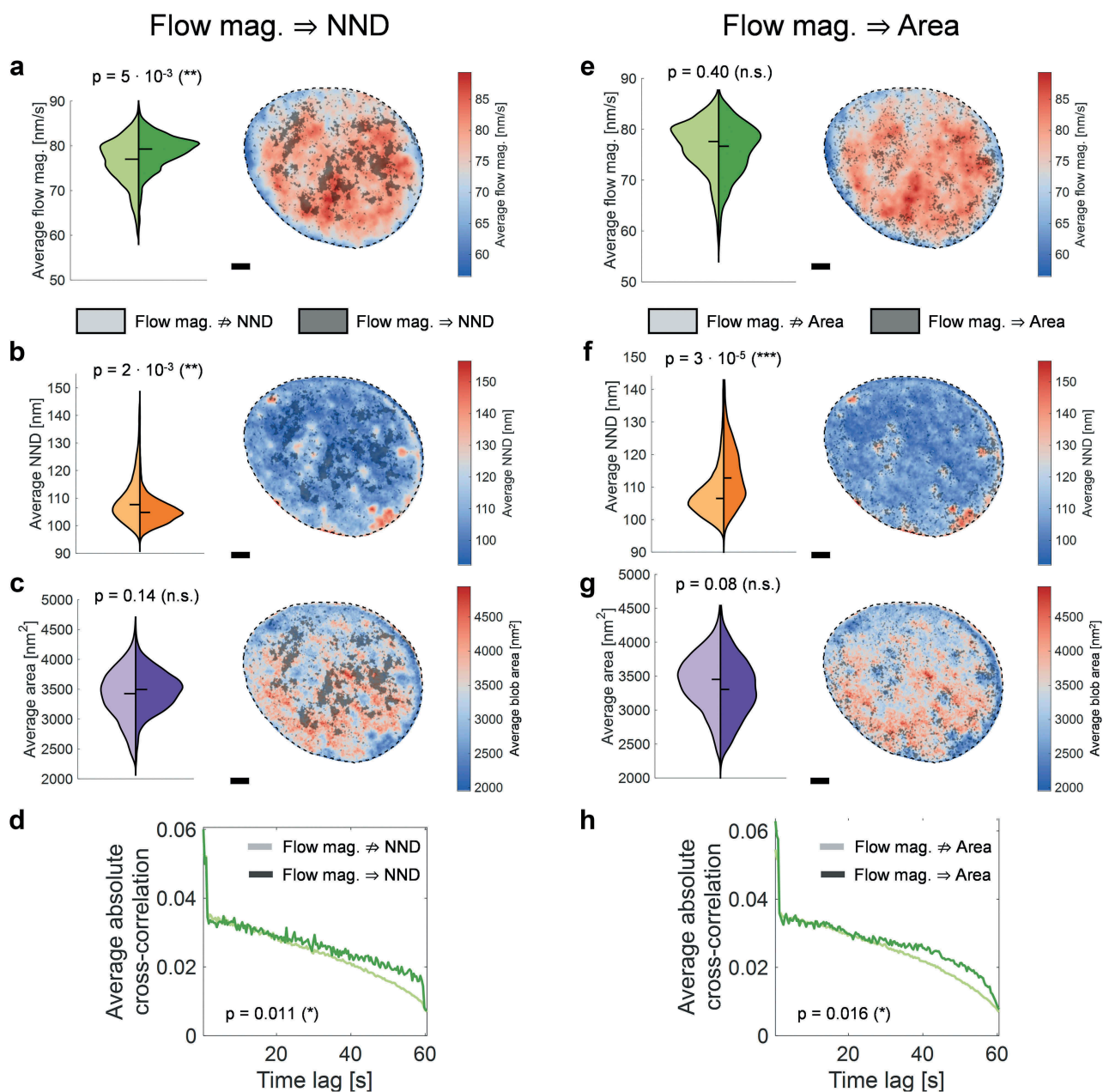
Figure 4. Enhanced dynamics and dense chromatin in regions with Granger causality. (a) The time-averaged flow magnitude across nuclear regions in which no Granger-causality was detected (bright color in the violin plot and the map on the right) and in regions in which the flow Granger-causes the NND of blobs. Scale bar is 3 μm. (b–c) The average NND and blob area in the same manner as for (a). (d) The average absolute cross-correlation between flow magnitude and NND for pixels in the two regimes (with/without Granger-causality). The correlation is significantly enhanced in the long-time limit for regions in which Granger-causality is detected. (e–h) As for (a–d) in the case of a detected Granger-causality from the flow magnitude to the blob area. Statistical significance was assessed using a Wilcoxon rank-sum test. The shown p-value is the median from 250 tests on sub-sampled data to avoid reporting a significance due to the large sample size alone.

under consideration could be evidenced (Supplementary Figure 2). Whenever a Granger-causal relationship from chromatin dynamics to a structural parameter was found, the temporal cross-correlation was slightly but significantly enhanced at very long time lags (Figure 4(d,h)),

indicating that the structure-dynamics coherence was sustained over an extended time in these regions. It should be noted that the size of chromatin blobs in relatively chromatin-void regions is likely to be well captured in our analysis due to a good signal-to-noise ratio, whereas in denser

chromatin regions multiple small but close chromatin blobs might be detected as merged into a single bigger blob. This artificially increases the measured blob surface area, while the NND is more robust to a blob merging effect in regions with high blob density (Supplementary Figure 3). The following discussion is therefore based only on the two more reliable parameters, blob dynamics and NND as a proxy for blob density.

In summary, we show that blob dynamics and blob structural parameters are strongly connected, and chromatin organization appears to arise as a consequence of chromatin dynamics. Such a cause-and-effect relationship can only be demonstrated in restricted areas of the nucleus, probably because stochasticity overrides deterministic mechanisms everywhere else. Strikingly, higher dynamics was found to be a cause for increased blob density (Figure 4; left column). Since biological experiments can only give access to a small subset of variables and influences, it should be kept in mind that the described causal relationships refer to the concept of Granger-causality. It is further possible that chromatin dynamics in itself is not the true cause here but instead a parameter closely linked to dynamics or the processes that generate dynamics, etc. The dynamics-structure Granger-causality described here can be further coupled via several additional unobserved factors. Below, we discuss a possible polymer-theoretical approach and different biological processes that (i) can induce chromatin dynamics beyond passive thermal or entropic contributions, (ii) could potentially give rise to the formation of transient chromatin blobs and (iii) could potentially explain how chromatin dynamics can shape the transient chromatin structure on the length scales of blobs.

Discussion

The inference of (Granger-) causality in complex systems provides a powerful tool to infer mechanisms from observations. Below we show that the results of our Granger-causality analysis are consistent with the theory of active semiflexible polymers. We discuss the major findings of simulations and analytical descriptions in a qualitative, intuitive way and describe the implications of this theory for the

organization and dynamics of chromatin. Finally, we assess if and under which circumstances chromatin blobs can be caused by an activity-induced motion of chromatin.

The theory of active semiflexible polymers may explain the existence of chromatin blobs

At the root of active polymers are active particles (self-propelling particles, dipolar motors, enhanced diffusion, etc.). These active particles can be either incorporated as part of the polymer itself (several monomers of the chain are active) or as part of the fluid surrounding a passive polymer (Figure 5(a)). These active particles are typically Active Effectors, which provide a local influx of energy by hydrolysis of ATP and associated chromatin remodeling or act by simply inducing deformation of the chromatin fiber upon binding. Variations between models yield qualitatively similar results [35], and since active effectors can act on the chromatin fiber in various ways, we shall neglect model-specific differences in this discussion.

Simulations and analytical approaches of active semiflexible polymers reveal that the diffusion of active polymers is enhanced compared to their passive counterpart [36–40]. The scaling behavior of the mean square displacement transits from a ballistic motion at very short time scales due to the particle propulsion to a subdiffusive regime at intermediate times and a diffusive regime at long time scales [41] (Figure 5(b)). Furthermore, the relaxation time of polymers, i.e. the time needed to recover to the initial conditions after applied stress, decreases with increasing activity [36]. In line with this observation, an active polymer also exhibits enhanced conformational fluctuations [40] and appears more flexible. In particular, the effective persistence length (the length over which a polymer is approximately stiff) of active polymers is decreased compared to their passive counterparts as a consequence of hairpin-formation [37].

The dependence of the relaxation time on the activity gives rise to interesting conformational properties of active polymers. The dimensionless Péclet number Pe, which is defined as the ratio of the (activity-induced) advection and (passive)
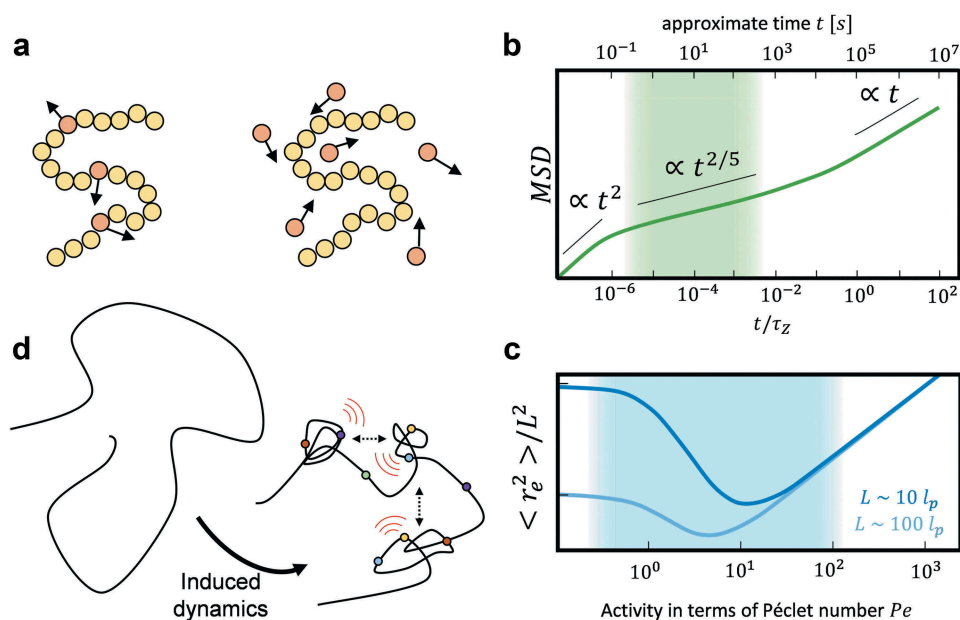
Figure 5. Dynamical and structural properties of active semiflexible polymers. (a) Active polymers can be described as polymers consisting of a mixture of passive (yellow) and active (red) monomers (left). Alternatively, active polymers are modeled as passive polymers embedded in a bath of active particles (right). Mathematically, a colored noise term can be included in the equations of motion to model activity [35]. (b) The mean squared displacement (MSD) of a linear active polymer with $L\tilde{1}0^5l_p$ at $Pe = 20$, subject to hydrodynamic interactions, is illustratively shown versus time lags in terms of the Zimm time τ_Z of a passive polymer (adapted from [54]). The upper x-axis shows an approximate mapping to absolute time in seconds (Supplementary Note 1) and the shaded area denotes the experimentally accessible time scale. The straight black lines serve as a guide to the eye to identify the different scaling regimes. (c) The mean squared end-to-end distance $\langle r_e^2 \rangle$ is shown illustratively for two polymers of length $L\tilde{1}0^1l_p$ (dark blue) and $L\tilde{1}0^2l_p$ (light blue) over the Péclet number Pe (adapted from [36]). The shaded area denotes the biologically relevant regime of the Péclet number (Supplementary Note 1). Ticks along the y-axis indicate one order of magnitude. D) According to the theory and simulations of active semiflexible polymers, dynamics induced by a host of chromatin players in distinct classes (i.e. polymerases, chromatin remodelers, topoisomerases, and HMG proteins) (colored dots) can stochastically induce the collapsing of a chromatin loop into a blob, and enhance blob–blob interactions. This would result in locally increased chromatin blob density and reduced blob nearest neighbor distances.

diffusion rate in a system (Supplementary Note 1), is commonly used to denote the activity strength in active polymers. For moderate activities as reflected by a low value of Péclet number Pe, the polymer experiences a significant shrinkage in terms of its means square end-to-end distance [36] and its radius of gyration [37]. For very large activities, however, it swells monotonically (Figure 5(c)). Shrinkage was also described in terms of a coil-to-globule-like transition upon increasing activity [42], which may be one reason why chromatin is well described by a fractal globule [43,44] with many-body contacts [45], that further displays anomalous diffusion [46]. Notably, however, the Péclet number might be as large as to cause the swelling of polymers in specific settings (Figure 5(c)).

The activity component in these models thus causes (i) enhanced conformational flexibility and diffusion with an intermediate subdiffusive regime and (ii) a shrinkage of polymers in specific regimes, which are determined by the activity and polymer characteristics such as its total length and its persistence length. We propose that the previously observed chromatin nanodomains/blobs [24,25,47] might be formed due to the local activity of various Active Effectors and that at least aspects of the dynamic and structural behavior of chromatin blobs can be captured by the theory of active semiflexible polymers (Figure 5(d)). This notion fits well with the findings that the blob dynamics and NND influence each other over space and time and that chromatin dynamics is at the root of blob organization (Figures 3 and 4). Below, we

consider biologically relevant and experimentally accessible time and length scales to evaluate if the theory of active semiflexible polymers can be united with experimental findings.

Experimentally and biologically relevant time and length scales of chromatin blob formation

Chromatin blobs were mainly observed on the length scale of tens [24,25,47] to hundreds [48] of nanometers. While most studies employed super-resolution microscopy on fixed samples, only two studies gave access to high-resolution chromatin dynamics using Structured Illumination Microscopy [48] and Deep-PALM imaging [24]. The time resolution in the latter was 360 ms, while images were acquired for up to 60 s. The experimentally accessible time range is thus in the order of $10^0 - 10^2$ seconds. Time in simulations is usually expressed by reference to the Zimm time τ_Z, which is of the order of 10^5s (Supplementary Note 1). Matching this time approximately to the simulated time scale for the dynamics of active polymers shows that only the subdiffusive regime is experimentally observable (shaded area in Figure 5(b)), which is in line with the subdiffusion of chromatin indeed measured in experiments [12,16,20,24,49].

The unit-less Péclet number *Pe*, defined as the ratio of advection and diffusion rate (Supplementary Note 1), conveys how much flow in a system depends on active animation rather passive diffusion. An upper bound on the diffusion constant of chromatin *in vivo* was estimated in the order of $D\tilde{1}0^{-3}\mu m^2/s^\alpha$ (ref. [20]). Taking into account the reported speed for processive enzymes such as transcribing RNA polymerase II or SMC proteins *in vitro*, the Péclet number was estimated to be between 0.1 and 100 for chromatin (Supplementary Note 1 for details of the estimation; the shaded area in Figure 5(c)). This range largely overlaps with the range where shrinkage is expected for chromatin segments, suggesting that active effector-induced activity may indeed contribute to the collapse of chromatin locally. It should be noted, however, that there are clearly local contexts, and exceptional time and length scales,

in which Péclet numbers can be as large as to cause polymers to swell, rather than shrink (Figure 5(c)).

The treatment of active circular polymers and polymer–polymer interactions can recapitulate experimental observations

The considerations above strongly suggest that the formation of chromatin blobs may be conceivably activity driven. The observation that changes in the nearest-neighbor distance of chromatin blobs can be frequently traced back to be caused by their dynamics (Figure 4(a–c)) further lends support to the theory. Area fluctuations of blobs for which their area is causally related to flow dynamics could reflect a growth/shrinkage of blobs according to the preceding dynamics (Figure 5(d)). Notably, that these blobs appear far from their closest neighbors opens up the possibility to track such blobs in three dimensions using Deep-PALM in the future to verify this hypothesis. Nevertheless, a direct translation of the theory of active semiflexible polymers to experimental data remains difficult due to the multitude of influences on chromatin that exist *in vivo*, and a number of possible additional mechanisms can be found in the literature. Considering structural elements of chromatin such as TADs and sub-TADs as well as chromatin loops such as those that can be extruded by SMC complexes [7,8], one should further take into account that chromatin blobs may at times correspond to sub-regions of quasi-circular, not of linear polymers. Such quasi-circular polymers may be stabilized by DNA bridging factors and/or SMC proteins at the loop bases [50] as well as a host of transcription factors operating as dimers. However, it is also likely that such circular structures would form in a highly dynamic and transient manner, as largely demonstrated for TADs, for instance, using a variety of techniques [4,51]. The results for linear active polymers are qualitatively transferable to circular ones [40], strengthening the hypothesis that blobs could correspond to loops or sub-TADs [24].

Activity was independently shown to enhance the looping probability of chromatin segments

[52]. Of note, there are hints that crowding may further promote blob formation in a crowder size- and concentration-dependent manner [53], and taking into account hydrodynamic interactions may result in even further shrinkage of polymers [54]. Interestingly, a simulation involving ensembles of active semiflexible polymers showed that the different polymers also get closer with increasing activity [38], suggesting that activity can enhance chromatin fiber density which may, in turn, promote blob formation. Furthermore, a clustering of active segments was observed upon 'switching on' activity of a subset of monomers of a chain, resulting in the segregation of active and inactive polymer regions reminiscent of chromatin blobs [55,56]. These computational results are in line with our observation that regions in which a high blob density is shown to depend on chromatin dynamics are also regions where dynamics is more elevated (Figure 4). Altogether it, therefore, appears that activity may promote both blob formation and blob–blob interactions both in a fiber and between fibers, by simultaneously enhancing blob mobility and decreasing the distance between blobs, possibly promoting, in turn, the collapsing of larger segments (Figure 5(d)).

Conclusions

Using a framework to infer Granger-causal relationships between spatio-temporal variables derived from a previous whole-chromatin live super-resolution imaging study [24], we analyzed if and how chromatin dynamics and organization influence each other. Within a subset of simultaneously observed variables in a system, this framework allowed us to pinpoint directed, Granger-causal relationships among parameters beyond the more conventional description of a basic correlation relationship. Within the limitations of our data set, we found that dynamics can be considered as a cause of structural parameters, and in particular that locally elevated chromatin dynamics causes blobs to be closer to each other. This is a rather counter-intuitive result as high chromatin density is commonly associated with closed chromatin, in which reduced chromatin density is expected due to

increased constraints on DNA. Our results suggest that closed chromatin is, in fact, a very active environment as further supported by the fact that a number of active effectors are known to be key determinants of closed chromatin assembly and function [10,57]. In addition, active processes have been shown experimentally [58,59] to drive coherent motion of chromatin [16,21]

To gain further insights into the existence of possible spatio-temporal causal relationships, the presented analysis may be extended to include the influence of variables at neighboring pixels. This is particularly important as chromatin blobs naturally move from frame to frame. However, since the number of regression parameter scales with the number of neighboring pixels (3 parameters × 10-time lags × 4 or 8 neighboring pixels = 120 to 240 parameters), the current length of the time series (166 data points) does not allow for reliable inference of causality including neighboring pixels. Further enhancing the time resolution of chromatin super-resolution imaging and circumventing photobleaching for longer acquisition may alleviate such restrictions in the future.

We demonstrate more broadly that the theory of active semiflexible polymers has the potential to explain the experimentally observed characteristics of chromatin blobs on biologically relevant scales, and can further provide an intuitive explanation for the observation that increased blob mobility can locally co-exist with dense chromatin. Blobs, as we are able to observe them, may nevertheless arise as a result of further stabilization by bridging and/or cross-linking factors. To probe this theory more explicitly, the analysis presented here may be carried out in cells that are depleted of certain key factors such as SMC proteins, heterochromatin players or ATP. In particular, a global loss of causality is expected in ATP-depleted cells.

Our analysis altogether reveals that chromatin dynamics is a key determinant of genome organization in nuclear space. However, such Granger-causality could be demonstrated only in restricted areas of the nucleus that are largely non-overlapping for distinct combinations of

parameters. The identification *per se* of Granger-causal relationships in a nucleus indicates that (multiple) deterministic molecular mechanisms likely exist that are responsible for chromatin organization. The sparsity of such Granger-causal relationships is however consistent with the idea that chromatin dynamics in nuclear space is largely dominated by stochasticity [60].

Author contributions

R. B. and H. A. S. designed the project; R. B. designed and carried out the data analysis; R. B. and H. A. S. interpreted results; H. A. S. supervised the project; R. B., G. F. and H. A. S. wrote the manuscript.

Disclosure statement

The authors declare no competing financial interest.

ORCID

Roman Barth http://orcid.org/0000-0002-5602-1164
Haitham A. Shaban http://orcid.org/0000-0002-0090-3301

References

[1] Rowley MJ, Corces VG. Organizational principles of 3D genome architecture. Nat Rev Genet. 2018;19 (12):789–800.

[2] Fourel G, Magdinier F, Gilson É. Insulator dynamics and the setting of chromatin domains. BioEssays. 2004;26:523–532.

[3] Nagano T, Lubling Y, Stevens TJ, et al. Single-cell Hi-C reveals cell-to-cell variability in chromosome structure. Nature. 2013;502:59–64.

[4] Finn EH, Pegoraro G, Brandão HB, et al. Extensive heterogeneity and intrinsic variation in spatial genome organization. Cell. 2019;176:1502–1515.e10.

[5] Nagano T, Lubling Y, Várnai C, et al. Cell-cycle dynamics of chromosomal organization at single-cell resolution. Nature. 2017;547:61–67.

[6] Dangkulwanich M, Ishibashi T, Liu S, et al. Complete dissection of transcription elongation reveals slow translocation of RNA polymerase II in a linear ratchet mechanism. Elife. 2013;2:e00971.

[7] Ganji M, Shaltiel IA, Bisht S, et al. Real-time imaging of DNA loop extrusion by condensin. Science. 2018;360:102–105.

[8] Davidson IF, Bauer B, Goetz D, et al. DNA loop extrusion by human cohesin. Science. 2019;366:1338–1345.

[9] Kong M, Cutts E, Pan D, et al. Human condensin I and II drive extensive ATP–dependent compaction of nucleosome–bound DNA. bioRxiv. 2019.

[10] McCauley MJ, Rueter EM, Rouzina I, et al. Single-molecule kinetics reveal microscopic mechanism by which High-Mobility Group B proteins alter DNA flexibility. Nucleic Acids Res. 2013;41(1):167–181.

[11] Friman ET, Deluz C, Meireles-Filho ACA, et al. Dynamic regulation of chromatin accessibility by pluripotency transcription factors across the cell cycle. Elife. 2019;8:e50087.

[12] Germier T, Kocanova S, Walther N, et al. Real-time imaging of a single gene reveals transcription-initiated local confinement. Biophys J. 2017;113:1383–1394.

[13] Gu B, Swigut T, Spencley A, et al. Transcription-coupled changes in nuclear mobility of mammalian cis-regulatory elements. Science. 2018;359(6379):1050–1055.

[14] Seeber A, Hauer MH, Gasser SM. Chromosome dynamics in response to DNA damage. Annu Rev Genet [Internet]. 2018;52:295–319. Available from: https://www.annualreviews.org/doi/10.1146/annurev-genet-120417-031334

[15] Nozaki T, Imai R, Tanbo M, et al. Dynamic organization of chromatin domains revealed by super-resolution live-cell imaging article dynamic organization of chromatin domains revealed by super-resolution live-cell imaging. Mol Cell. 2017;10:1–12.

[16] Zidovska A, Weitz DA, Mitchison TJ. Micron-scale coherence in interphase chromatin dynamics. Proc Natl Acad Sci U S A. 2013;110:15555–15560.

[17] Zada D, Bronshtein I, Lerer-Goldshtein T, et al. Sleep increases chromosome dynamics to enable reduction of accumulating DNA damage in single neurons. Nat Commun. 2019;10(1). DOI:10.1038/s41467-019-08806-w

[18] Nagashima R, Hibino K, Ashwin SS, et al. Single nucleosome imaging reveals loose genome chromatin networks via active RNA polymerase II. J Cell Biol. 2019;218(5):1511–1530.

[19] Shaban HA, Seeber A. Monitoring the spatio-temporal organization and dynamics of the genome. Nucleic Acids Res. 2020;48(7):3423–3434.

[20] Shaban HA, Barth R, Bystricky K. Hi-D: nanoscale mapping of nuclear dynamics in single living cells. Genome Biol. 2020;21. DOI:10.1186/s13059-020-02002-6

[21] Shaban HA, Barth R, Bystricky K. Formation of correlated chromatin domains at nanoscale dynamic resolution during transcription. Nucleic Acids Res [Internet]. 2018;46:e77.

[22] van Steensel B, Furlong EEM. The role of transcription in shaping the spatial organization of the genome. Nat Rev Mol Cell Biol. 2019. DOI:10.1038/s41580-019-0114-6

[23] Zheng H, Xie W. The role of 3D genome organization in development and cell differentiation. Nat Rev Mol Cell Biol. 2019;20:535–550.

[24] Barth R, Bystricky K, Shaban HA. Coupling chromatin structure and dynamics by live super-resolution imaging. Sci Adv 2020; DOI: 10.1126/sciadv.aaz2196, In press.

[25] Ricci MA, Manzo C, García-Parajo MF, et al. Chromatin fibers are formed by heterogeneous groups of nucleosomes in vivo. Cell. 2015;160:1145–1158.

[26] Welf ES, Danuser G. Using fluctuation analysis to establish causal relations between cellular events without experimental perturbation. Biophys J. 2014;107:2492–2498.

[27] Duronio RJ, O'Farrell PH, Sluder G, et al. Sophisticated lessons from simple organisms: appreciating the value of curiosity-driven research. Dis Model Mech. 2017;10:1381–1389.

[28] Granger CWJ. Investigating causal relations by econometric models and cross-spectral methods. Econometrica. 1969;37:424.

[29] Nehme E, Weiss LE, Michaeli T, et al. Deep-STORM: super-resolution single-molecule microscopy by deep learning. Optica [Internet]. 2018;5:458–464. Available from: http://www.osapublishing.org/optica/abstract.cfm?URI=optica-5-4-458

[30] Diebold FX, Mariano RS. Comparing predictive accuracy. J Bus Econ Stat. 1995; 13(3):253–63.

[31] Guitton H, Theil H. Economic forecasts and policy. Rev économique. 1963;14:163.

[32] Papagiannopoulou C, Miralles DG, Demuzere M, et al. Global hydro-climatic biomes identified via multitask learning. Geosci Model Dev. 2018;11:4139–4153.

[33] Ando RK, Zhang T. A framework for learning predictive structures from multiple tasks and unlabeled data. J Mach Learn Res. 2005;6:1817–1853.

[34] Byrd RH, Hansen SL, Nocedal J, et al. A stochastic quasi-newton method for large-scale optimization. SIAM J Optim. 2016;26:1008–1031.

[35] Winkler RG, Elgeti J, Gompper G. Active polymers — emergent conformational and dynamical properties: a brief review. J Phys Soc Jpn. 2017;86:101014.

[36] Eisenstecken T, Gompper G, Winkler RG. Conformational properties of active semiflexible polymers. Polymers (Basel). 2016;8:304.

[37] Foglino M, Locatelli E, Brackley CA, et al. Non-equilibrium effects of molecular motors on polymers. Soft Matter. 2019;15:5995–6005.

[38] Loi D, Mossa S, Cugliandolo LF. Non-conservative forces and effective temperatures in active polymers. Soft Matter. 2011;7:10193.

[39] Ghosh A, Gov NS. Dynamics of active semiflexible polymers. Biophys J. 2014;107:1065–1073.

[40] Mousavi SM, Gompper G, Winkler RG. Active Brownian ring polymers. J Chem Phys. 2019;150:064913.

[41] Eisenstecken T, Gompper G, Winkler RG. Internal dynamics of semiflexible polymers with active noise. J Chem Phys. 2017;146(15):154903.

[42] Bianco V, Locatelli E, Malgaretti P. Globulelike conformation and enhanced diffusion of active polymers. Phys Rev Lett. 2018;121(21). DOI:10.1103/PhysRevLett.121.217802

[43] Mirny LA. The fractal globule as a model of chromatin architecture in the cell. Chromosome Res. 2011;19:37–51.

[44] Lieberman-Aiden E, van Berkum NL, Williams L, et al. Comprehensive mapping of long-range interactions reveals folding principles of the human genome. Science. 2009;326:289–293.

[45] Polovnikov KE, Nechaev S, Tamm MV. Many-body contacts in fractal polymer chains and fractional Brownian trajectories. Phys Rev E. 2019;99. DOI:10.1103/PhysRevE.99.032501

[46] Tamm MV, Nazarov LI, Gavrilov AA, et al. Anomalous diffusion in fractal globules. Phys Rev Lett. 2015;114(17). DOI:10.1103/PhysRevLett.114.178102

[47] Xu J, Ma H, Jin J, et al. Super-resolution imaging of higher-order chromatin structures at different epigenomic states in single mammalian cells. Cell Rep. 2018;24(4):873–882.

[48] Miron E, Oldenkamp R, Pinto DMS, et al. Chromatin arranges in filaments of blobs with nanoscale functional zonation. bioRxiv. 2019;566638.

[49] Chen B, Gilbert LA, Cimini BA, et al. Dynamic imaging of genomic loci in living human cells by an optimized CRISPR/Cas system. Cell. 2013;155:1479–1491.

[50] Gutierrez-Escribano P, Newton MD, Llauró A, et al. A conserved ATP- and Scc2/4-dependent activity for cohesin in tethering DNA molecules. Sci Adv. 2019;5: eaay6804.

[51] Beagrie RA, Scialdone A, Schueler M, et al. Complex multi-enhancer contacts captured by genome architecture mapping. Nature. 2017;543:519–524.

[52] Shin J, Cherstvy AG, Kim WK, et al. Facilitation of polymer looping and giant polymer diffusivity in crowded solutions of active particles. New J Phys. 2015;17:113008.

[53] Cao X, Zhang B, Zhao N. Crowding-activity coupling effect on conformational change of a semi-flexible polymer. Polymers (Basel). 2019;11:1021.

[54] Martín-Gómez A, Eisenstecken T, Gompper G, et al. Active Brownian filaments with hydrodynamic interactions: conformations and dynamics. Soft Matter. 2019;15:3957–3969.

[55] Smrek J, Chubak I, Likos CN, et al. Active topological glass. Nat Commun. 2020;11:26.

[56] Smrek J, Kremer K. Small activity differences drive phase separation in active-passive polymer mixtures. Phys Rev Lett. 2017;118:098002.

[57] Xue Y, Pradhan SK, Sun F, et al. Mot1, Ino80C, and NC2 function coordinately to regulate pervasive transcription in yeast and mammals. Mol Cell. 2017;67:594–607.e4.

[58] Saintillan D, Shelley MJ, Zidovska A. Extensile motor activity drives coherent motions in a model of interphase chromatin. Proc Natl Acad Sci U S A. 2018;115:11442–11447.

[59] Bruinsma R, Grosberg AY, Rabin Y, et al. Chromatin hydrodynamics. Biophys J. 2014;106:1871–1881.

[60] Lorenz EN. Deterministic Nonperiodic Flow. J Atmos Sci. 1963;20:130–141.